Construction and Building Materials 220 (2019) 701–711

Contents lists available at ScienceDirect

Construction and Building Materials

journal homepage: www.elsevier.com/locate/conbuildmat

Special Issue
CICE 2018 - FRP composites in construction: Advances in material research & engineering

Effect of the EBROG method on strip-to-concrete bond behavior

Amir Tajmir-Riahi [a], Niloufar Moshiri [a,b,*], Christoph Czaderski [b], Davood Mostofinejad [a]

[a] Isfahan University of Technology (IUT), Isfahan, Iran
[b] Swiss Federal Laboratories for Materials Science and Technology (Empa), Überlandstrasse 129, 8600 Dübendorf, Switzerland

HIGHLIGHTS

- Affirming the efficiency of EBROG method to bond the precured CFRP strips to concrete structure.
- A two-fold increase in bond strength of EBROG joints compared to that of EBR joints.
- Proposing an experimental-analytical model to predict bond strength of CFRP strips-to-concrete.
- Utilizing a digital image analysis (DIC) measurement system to determine full-filed deformations.

ARTICLE INFO

Article history:
Received 8 April 2019
Received in revised form 14 May 2019
Accepted 7 June 2019
Available online 24 June 2019

Keywords:
EBROG
Externally bonded reinforcement on grooves
FRP
DIC
Side-view measurement

ABSTRACT

The bond behavior of precured FRP strips and steel plates to concrete substrate was investigated in this research in terms of the load capacity, slip and strain distribution and debonding mechanism. Experimental single lap shear tests were performed and an experimental-analytical model was proposed to determine the bond strength of the FRP-bonded joints. Two strengthening methods, including externally bonded reinforcement (EBR) and externally bonded reinforcement on groove (EBROG), were compared. A two-dimensional digital image correlation (2D-DIC) system was utilized to measure the full-field deformations.

Compared to the 90 mm effective bond length for the EBR method, the effective bond lengths for the EBROG method were equal to 145 and 160 mm for 5×5 and 5×10 mm groove cross sections, with 92% and 112% higher loads, respectively. In addition, the results showed that the EBROG method improved the bond resistance of steel-to-concrete joints, but it was not as efficient as it was for the FRP-to-concrete bonded joints. Furthermore, the crack propagation underneath the strip was assessed for the first time for the EBROG method, by using a side-view measurement.

1. Introduction

FRP composites have been accepted extensively for retrofitting and strengthening civil structures, i.e., buildings and bridges. Proper bond behavior between FRP and concrete is important for the strengthening efficiency. Usually, premature debonding happens before full capacity of the materials is achieved. Therefore, the bond behavior of FRP composites to concrete substrate has been studied over the past decades [1–5]. Experimental, analytical, and numerical research works were performed to evaluate the effect of different parameters [6–10]. Design equations were also proposed to predict bond behavior [1,11–13]. Efforts have been made to postpone debonding, which achieves higher bond resistance. Among those efforts, the EBROG method was introduced as a substitute for the EBR method at Isfahan University of Technology (IUT) [14]. Flexural strengthening of concrete beams with FRP composites using the EBROG method demonstrated a high increase in the beam load capacity and postponed the debonding [14,15]. A comparison of the EBROG method with the conventional EBR technique in the axial/flexural retrofitting of columns, in the shear/flexural strengthening of reinforced concrete beams, and in the repair of beam-column joints was investigated through previous research works [16–21]. The bond behavior of FRP sheets-to-concrete was examined by Mostofinejad et al. [22–26]. The influences of the groove characteristics, bond length, concrete properties, loading rate, and mixed-mode I/II loading were

* Corresponding author at: Swiss Federal Laboratories for Materials Science and Technology (Empa), Überlandstrasse 129, 8600 Dübendorf, Switzerland.
E-mail address: niloufar.moshiri@cv.iut.ac.ir (N. Moshiri).

https://doi.org/10.1016/j.conbuildmat.2019.06.065
0950-0618/

surveyed [22–25]. Significant improvement in the bond behavior was well approved when the EBROG method was used, which resulted in a tremendous increase in the bond resistance, postponement of the debonding of FRP sheets from concrete substrate or, in some cases, FRP tensile rupture instead of debonding; and higher slip and strain values that could be developed in the FRP.

Previously, the EBROG method was well investigated for the bond behavior of FRP sheets (carbon or glass fibers) [22,24,25,27,28]. The effect of the EBROG method on the bond behavior of precured FRP strips, which have a much higher load capacity compared to that of the FRP sheets was studied in this research work. For this purpose, an experimental and analytical program was directed. Single lap shear tests on FRP strips-to-concrete bonded joints were performed. Unidirectional precured carbon FRP strips of 1.4 mm thickness were used to strengthen concrete blocks. According to the experimental results and by considering the failure modes, a model was proposed to predict the bond strength of FRP-to-concrete. To examine the efficiency of the EBROG method on higher bond capacities, the steel plate-to-concrete bond behavior was also assessed. Lap shear tests on steel-to-concrete bonded joints had similar configurations to that of FRP-strengthened joints but were strengthened with 5 mm-thick steel plates.

It is worth mentioning that current paper is an extended version of the authors' paper that was presented at the CICE2018 conference [29]. The lap shear experiments on FRP-to-concrete bonded joints were presented in a paper by authors [30]. Additional results, with respect to that paper, are discussed in the current paper to approach a thorough understanding of the EBROG method and proposing an experimental-analytical model to evaluate the bond strength of FRP strips-to-concrete. In addition to FRP-to-concrete bonded joints, steel-to-concrete joints are also presented in current paper. An innovative side-view measurement is presented as well.

2. Experimental program

2.1. Material properties

Single lap shear tests were performed to investigate the bond behavior of strips to concrete. Concrete blocks with $150 \times 150 \times 350$ mm dimensions were casted, all with a same concrete batch, and strengthened with precured carbon FRP strips and steel plates. Compressive strength of concrete blocks, which were determined by three standard 100×200 mm cylinders, were 38.20 MPa with a standard deviation of 1.04 at the lap shear testing time.

Unidirectional carbon FRP (CFRP) strips, called Sika CarboDur S514, were utilized to strengthen specimens number 1–6. According to the manufacturer's data sheet, precured CFRP strips had a thickness of 1.4 mm, width of 50 mm, elastic modulus of 165 GPa, ultimate tensile strength of 2800 MPa, and ultimate tensile strain of 1.7%. CFRP strips were bonded to the concrete substrate over a bond length of 240 mm by means of a two-part epoxy adhesive named Sikadur 31. The adhesive had a modulus of elasticity that was equal to 4.3 GPa, with a tensile strength of 15–20 MPa, according to the manufacturer's data sheet. It is worth mentioning that the bonded length started 55 mm away from the concrete edge to prevent stress concentration at the loaded end.

To briefly study the effect of the EBROG method when steel plates were used for strengthening, four steel-to-concrete bonded joints were tested. In contrast to the FRP materials properties, the steel plates mechanical properties had to be determined by performing coupon tests; since no data sheet presenting the steel properties were available by the producer company. The steel mechanical properties, which are reported in Table 1, were determined by the tensile test on three standard samples with 5 mm thickness and 12.5 mm width, according to ASTM E8 [31] (Fig. 1). Steel plates with a thickness of 5 mm, elastic modulus of 204 GPa, yield tensile strength of 458 MPa, and ultimate tensile strength of 552 MPa were utilized in specimens number 7–11.

2.2. Specimen preparation

The two methods, EBR and EBROG, were used to strengthen the concrete blocks for lap shear tests. In EBR, the surface preparation was performed as follows: removing a thin weak layer of concrete surface by a grinding machine and cleaning the dust from the surface by means of compressed air. Grinding the surface was executed to remove a thin layer of concrete with a thickness of approximately 1–2 mm in a way that the weak surface layer of concrete was removed and the aggregates were exposed. The strip was then bonded to the substrate by using an epoxy adhesive (Fig. 2). In EBROG, no surface preparation was performed. Instead, two longitudinal grooves with the defined (target) dimension in the cross section and with 20 mm free distance perpendicular to the groove direction were cut in the concrete substrate. The selected dimensions of the groove cross section that were studied in current research was 5×5, 5×10 or 10×10 mm, and can be found for each specimen in Table 2. Cleaning the substrate with compressed air, totally filling the grooves with epoxy adhesive, and, finally, adhering the strip over the grooves were the steps for preparing the EBROG joint (Fig. 2). After seven days of curing, the specimens were tested in the testing machine.

2.3. Testing method

Single lap shear tests were conducted using a 300 kN hydraulic jack at the Isfahan University of Technology (IUT). The tensile load was applied on one end of the strip in displacement-controlled mode with a rate of 2 mm/min (according to ASTM D3039 [32]). The strip

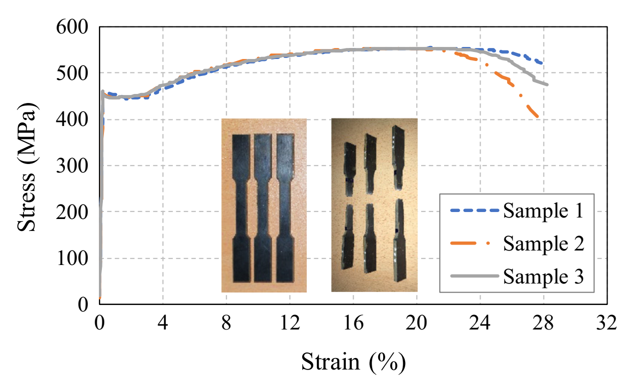

Fig. 1. Results of steel coupon tests.

Table 1
Steel coupon tensile tests.

Sample	Yield strength (MPa)	Ultimate tensile strength (MPa)	Elongation (%)	Modulus of elasticity (GPa)
1	459	553	28	201
2	456	550	27	210
3	458	552	28	200

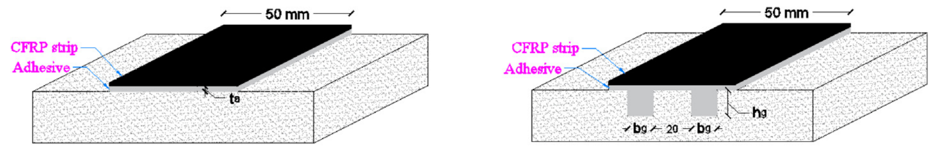

(a) EBR method (b) EBROG method

Fig. 2. Strengthening methods; (a) EBR method; (b) EBROG method.

Table 2
Test layout and experimental results.

Specimen No.	Specimen label	Strengthening method	Strengthening strip	Groove width, b_g (mm)	Groove depth, h_g (mm)	Front/ Side-view measurement	Bond strength, P_u (kN)	$P_u/P_{u,Avg\_EBR}$	Failure mode, debonding in:
1	EBR-1	EBR	CFRP strip	–	–	Front	25.29	–	Concrete
2	EBR-2	EBR	CFRP strip	–	–	Front	23.70	–	Concrete
3	EBROG-5 × 5-1	EBROG	CFRP strip	5	5	Front	47.14	1.92	Adhesive
4	EBROG-5 × 5-2	EBROG	CFRP strip	5	5	Front	32.41*	–	Adhesive
5	EBROG-5 × 10-1	EBROG	CFRP strip	5	10	Front	52.66	2.15	Adhesive
6	EBROG-5 × 10-2	EBROG	CFRP strip	5	10	Front	51.40	2.10	Adhesive
7	EBR-steel-1	EBR	Steel plate	–	–	Front	70.14	–	Concrete
8	EBR-steel-2	EBR	Steel plate	–	–	Front	68.97	–	Concrete
9	EBROG-10 × 10-steel-1	EBROG	Steel plate	10	10	Front	84.73	1.22	Steel-adhesive interface
10	EBROG-10 × 10-steel-2	EBROG	Steel plate	10	10	Front	90.72	1.30	Deep concrete
11	EBROG-10 × 10-steel-3	EBROG	Steel plate	10	10	Side	74.89	1.08	Adhesive

Notes: P_{u,Avg_EBR} = The average of the results of two similar EBR joints.
*Premature failure due to sliding of the strip in the clamps during the test.

end was tightly fixed in clamps and held by a 350 kN hydraulic jack during the test. The pulling force was measured by a 300 kN load cell and was recorded by a digital data logger. The test instrumentation and coordinate axis system are shown in Fig. 3.

A two-dimensional digital image correlation (2D-DIC) system was utilized to measure the full-field deformations in the specimen surface. Deformations were measured by tracking the displacements on a textured-surface through successive images. To do so, the specimen surface was painted white, and a colorful pattern with red, blue and green spots was produced on the surface. Digital images were captured by using a Nikon D5200 digital camera with 36 megapixel resolution and a Nikkor (18–135 mm) lens. The specimen surface was illuminated by two white light projectors to minimize the light noise. Images were taken manually without a distinct time interval. The stages at which each image was taken can be distinguished from the visible points on load-slip diagrams (Fig. 5); each point refers to a stage. The measurement field was 150 × 350 mm in size, in which subsets of 250 × 250 pixels (approximately 17 × 17 mm) with 16 pixel spacing were generated [33]. Deformations were calculated by using the particle image velocimetry (PIV) method with GeoPIV8 software [16,30,34].

2.4. Test layout

Details about the specimens are presented in Table 2. The specimens' labels start with the name of the strengthening method, i.e., the EBR or EBROG method. For the EBROG joints, the groove dimensions are stated afterwards. In the specimens strengthened with a steel plate, the name of "steel" was then added to the labels. Finally, number 1 or 2 was added to show the repetition of identical tests. (It is worth mentioning that the FRP-to-concrete joints labels were similar to those of the other authors' paper [30], for the sake of conformity and easiness.) Specimens number 1–6 were retrofitted with FRP strips via the EBR or EBROG method. Specimens number 7–11 were strengthened with steel plates through the EBR or EBROG method. In tests number 1–10, the whole front

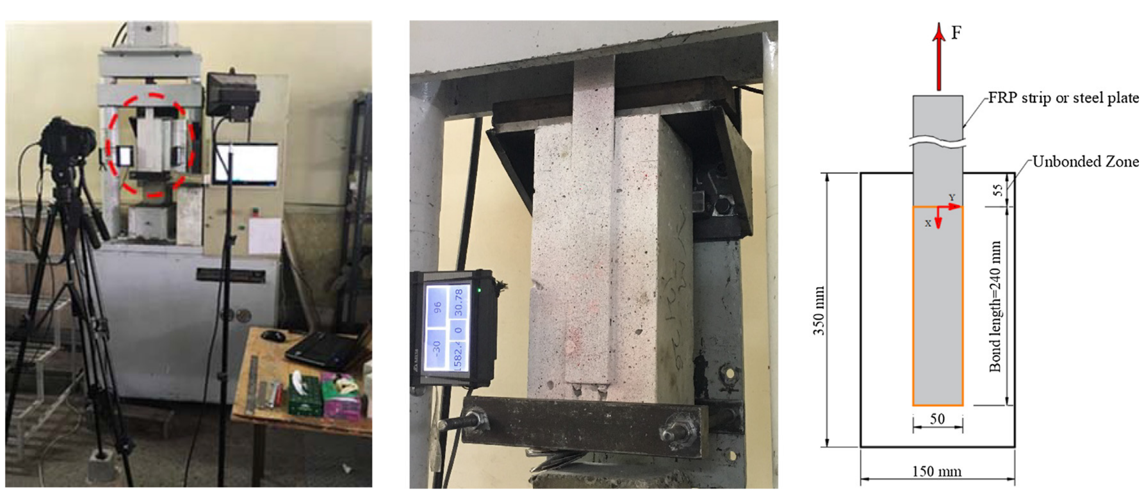

Fig. 3. Test instrumentation.

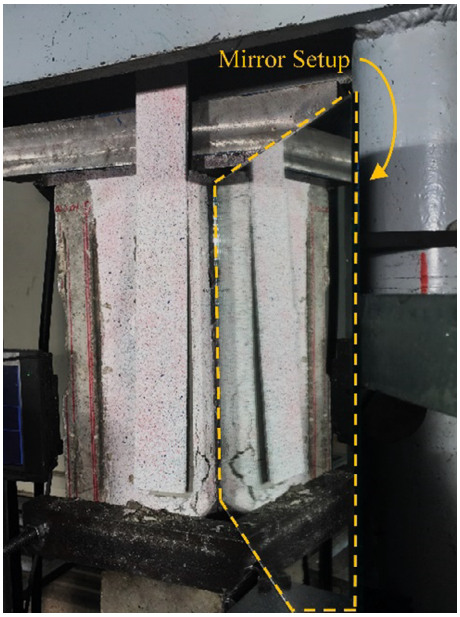

Fig. 4. Test setup for side-view measurement (the photo was taken after failure for better perception of the setup).

view of the specimen was captured, and deformations were measured with DIC.

2.5. Side-view measurement

Assessing the deformations and crack propagation underneath the EBROG bonded joint was conducted for the first time in current research. In other words, the deformations, strains and crack propagation were evaluated deep inside the concrete, beneath the strip. In specimen number 11, side-view measurements with 2D-DIC were performed with an innovative technique to monitor the field.

In specimen number 11, the steel plate was bonded at the longitudinal edge of the concrete block so that the surrounding concrete existed on one border of the steel plate (in specimens 1–10, both sides of the strip outside its borders were confined with surrounding concrete). The specimen configuration and test setup for this side-view measurement are represented in Fig. 4. Due to the testing machine setup, it was not possible to position the specimen in a way that the side view of the specimen, i.e., beneath the strip, could be monitored with a digital camera. Therefore, an innovative technique was utilized to observe the side view of the specimen. A mirror positioned 45 degrees with respect to the specimen's front-view was installed close to the concrete block. When looking at the front-view of the specimen, the side-view was also visible in the mirror, thus, the images taken from the front-view of the specimen could also capture the side-view. With this innovative technique, measuring both the side and front views was feasible by using only one camera. Although this technique is not a full 3D DIC system and needs improvement to minimize the errors and modify the measurements, it could be referred to as a semi-3D DIC system. Therefore, only qualitatively (and not quantitatively) crack pattern developments are presented for this measurement in this paper.

3. Experimental results

3.1. FRP-to-concrete bonded joints

3.1.1. Bond strength

It can be observed in Table 2 that the bond strengths of the EBR joints were 25.29 and 23.70 for the two repetitions. The EBROG joints, however, achieved much higher bond resistance. Specimens "EBROG-5 × 5-1," "EBROG-5 × 10-1," and "EBROG-5 × 10-2" experienced 47.14, 52.66, and 51.40 kN bond capacity, which indicated factors of 1.92, 2.15 and 2.10 compared to that of EBR joints, respectively. Therefore, a two-fold increase in the bond strength was concluded when the EBROG method was used. Moreover, bigger groove dimensions resulted in higher bond resistance. Transferring the interfacial shear stresses deep into the concrete substrate, which is confined by the surrounding concrete, contributed to an increased bond strength in the EBROG method. It is worth mentioning that specimen "EBROG-5 × 5-2," showed premature failure during the test due to the sliding of the strip in the end clamps and, therefore, was removed from the results section.

3.1.2. Load-slip behavior

The strip longitudinal displacement relative to the concrete substrate is called slip. Subtracting the average value of the concrete deformation from the strip deformation in its central section results in slip. The load-slip behavior of tested specimens is plotted in Fig. 5. It can be observed that the EBR joints had a typical bilinear behavior that turned into a horizontal branch at the stage of initiation of the debonding. In contrast, EBROG joints demonstrated an ascending behavior with a variable decreasing slope.

At much higher slip values, the load-slip behavior of the EBROG joints turned horizontal. The corresponding point was selected as the stage of initiation of debonding beyond which no considerable increase in the load was experienced. After the point of "initiation of debonding," the CFRP strip is completely separated over a part of

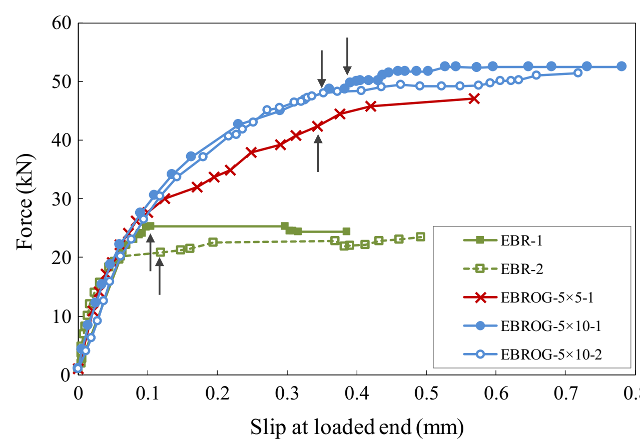

Fig. 5. Load-slip behavior of FRP-to-concrete bonded joints (arrows specify the load stages that are shown in Fig. 6).

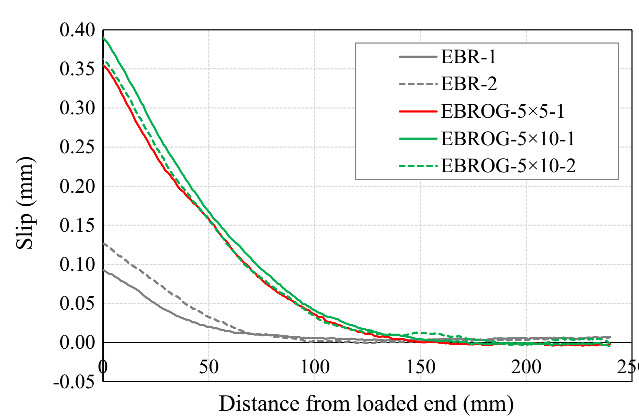

Fig. 6. Slip distribution at the initiation of debonding for FRP-to-concrete joints.

the bond length, and the shear stress is zero; therefore, the measured slip in this area is no longer of interest. The slip distribution along the bond length at the initiation of debonding was plotted for the specimens that are shown in Fig. 6. FRP-strengthened specimens using the EBR method experienced slip of 0.10 and 0.12 mm at the loaded end. On the other hand, using the EBROG method led to higher slips of 0.38, 0.4 and 0.36 mm for specimens "EBROG-5 × 5-1," "EBROG-5 × 10-1" and "EBROG-5 × 10-2," respectively; however, the load was much higher. In addition, the average effective bond lengths were 90, 145 and 160 mm for EBR specimen, EBROG specimen with 5 × 5 grooves and EBROG joint with 5 × 10 mm grooves, respectively. The EBROG method transferred the load over a longer bond length, which was slightly higher for deeper grooves.

3.1.3. Slip evolution

The slip distribution along the bond length during the test is exhibited in Fig. 7. Successive images were taken from the specimen manually without a distinct load/time increment between them. Slip propagation was demonstrated very well in the slip distribution diagrams, which indicated that longer bond length experienced slip as the test continued. In the EBR specimens, the stage of initiation of debonding can be easily distinguishable in Fig. 7. Significant increase in the slip and a large gap between the consecutive slip diagrams correspond to the initiation of debonding in the EBR specimens. However, the EBROG joints demonstrated sequential uninterrupted diagrams from which the initiation of debonding could not be easily observed. Therefore, the load-slip diagrams were considered to determine this stage.

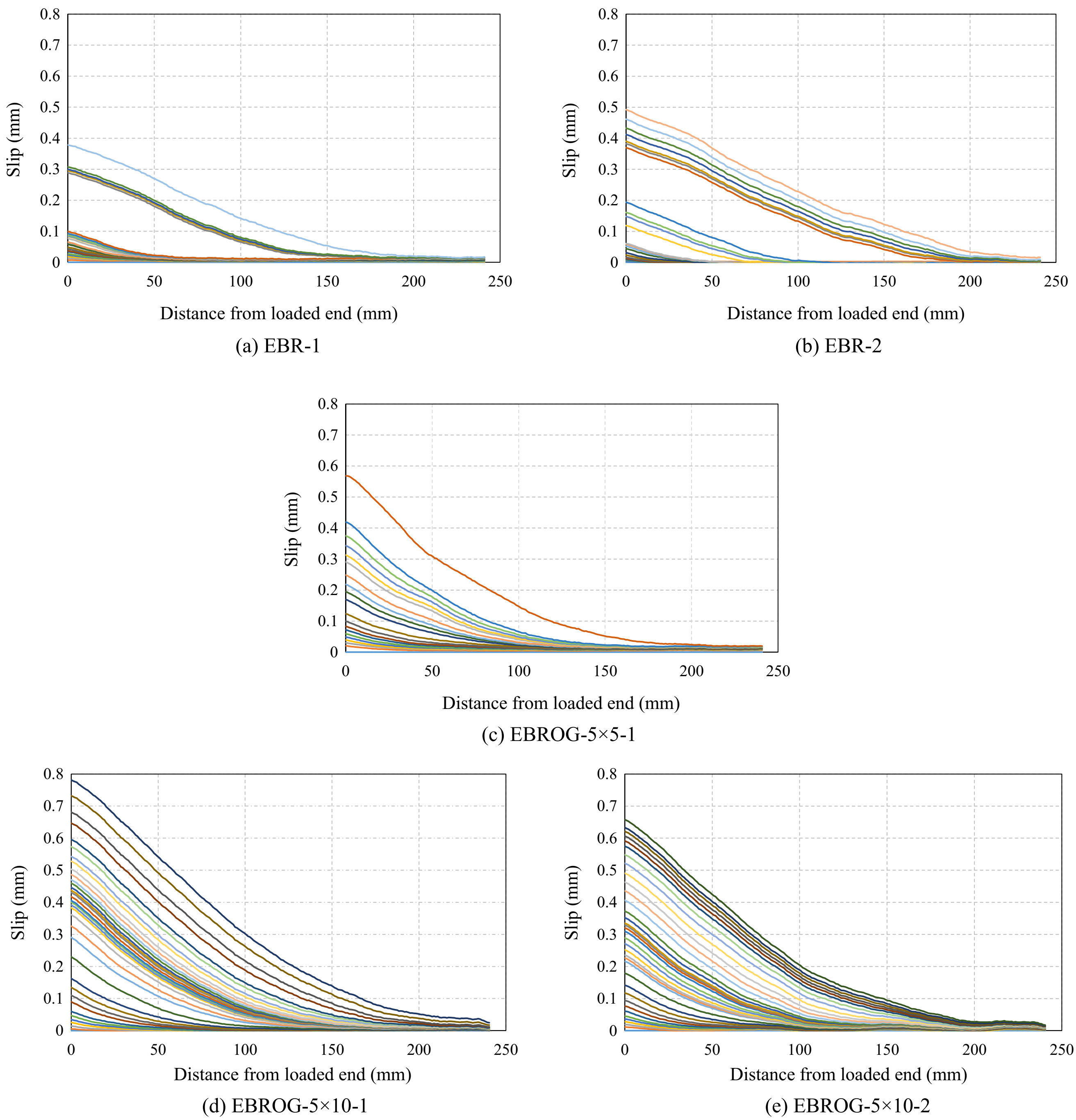

Fig. 7. Slip distribution of FRP-to-concrete bonded joints during loading (bond length = 240 mm).

3.1.4. Strain distribution and failure mode

By exploiting the DIC system, the strain field could be determined in the whole field. In Fig. 8, the strain distribution is demonstrated at the stage of initiation of debonding and in the final stage. It was observed that at the stage of initiation of debonding, the strain developed from the starting point of the bond, up to a certain length, which is the effective bond length for each specimen. For example, in specimens "EBR-1" and "EBR-2," the effective bond length that experienced strain at the initiation of debonding was approximately 90 mm. It is also observed in Fig. 8 that the effective bond length of EBROG specimens was higher compared to that of the EBR specimen. Approximately 145 and 190 mm bond length can be concluded in that figure for EBROG specimens with 5 × 5 and 5 × 10 mm grooves.

By comparing Strain distribution at initiation of debonding and at final stage in Fig. 8, it can be seen that the field on FRP which was experiencing the highest strain (red color in the color bar is related to the highest strain in these figures), was moved from top of the strip to its middle. It means that the highest strain took place in another position further from the loaded end. In other words, as the debonding propagated, the strain field developed along the strip length, and the point corresponding to the maximum strain went further. Meanwhile, the loaded end was debonded from the concrete and debonding propagated along the strip. This observation agrees well with the propagation of interfacial shear stress along the strip length.

It is noteworthy that the bottom left value on the blue monitor in these graphs demonstrates the force in the kg.f unit and should be converted to the kN unit.

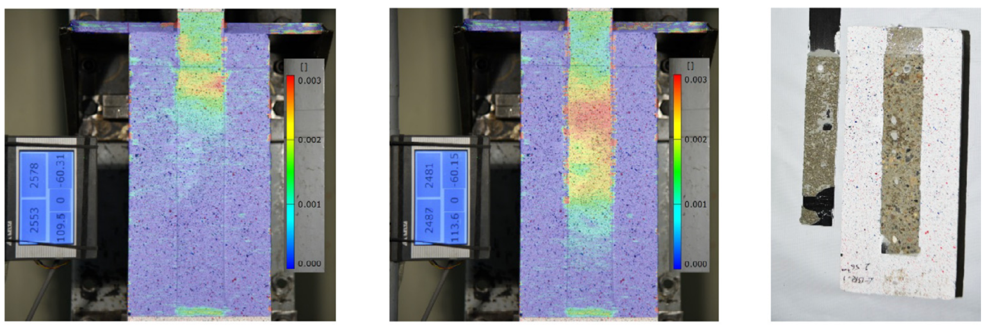

Strain distribution at initiation of debonding | Strain distribution at final stage | Failure mode

(a) "EBR-1"

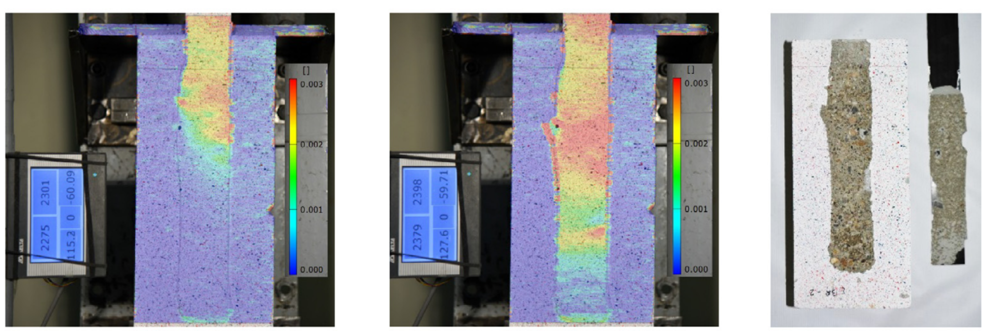

Strain distribution at initiation of debonding | Strain distribution at final stage | Failure mode

(b) "EBR-2"

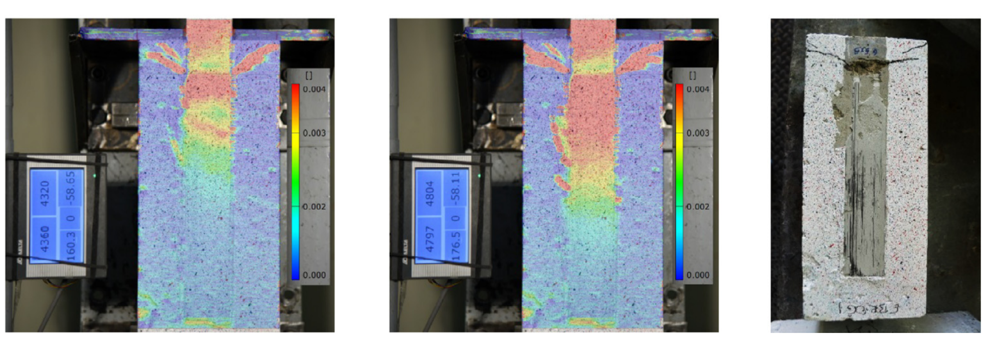

Strain distribution at initiation of debonding | Strain distribution at final stage | Failure mode

(c) "EBROG-5×5-1"

Fig. 8. Strain distribution and failure modes of FRP-to-concrete bonded joints.

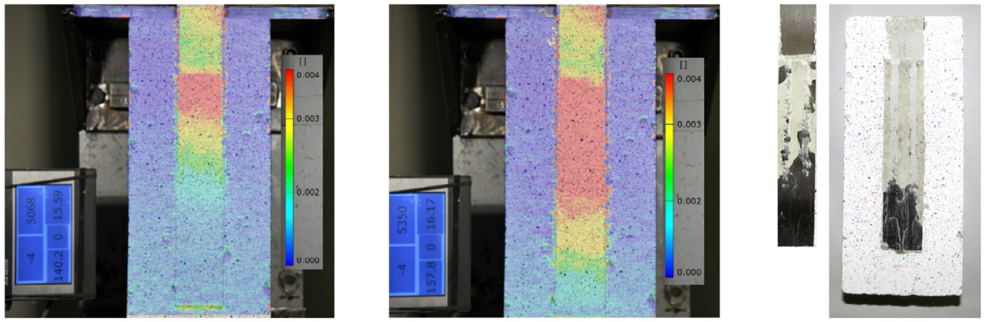

Strain distribution at initiation of debonding | Strain distribution at final stage | Failure mode

(d) "EBROG-5×10-1"

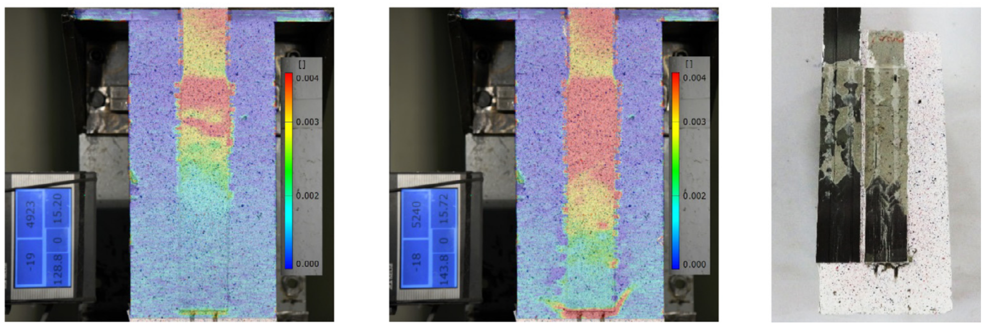

Strain distribution at initiation of debonding | Strain distribution at final stage | Failure mode

(e) "EBROG-5×10-2"

Fig. 8 (*continued*)

The failure mode of FRP-strengthened blocks is also shown in Fig. 8. The failure mode of EBR specimens was debonding in the concrete, as expected. In contrast, the EBROG joints experienced debonding in the adhesive layer, which is called cohesive failure. Concrete substrate was, therefore, not the weakest constituent in the FRP/epoxy/concrete system. The EBROG method helped the joint to postpone the debonding by stiffening the concrete substrate. Although partly interface failure inside the strip was observed at the end of the bond zone, this phenomenon is considered to be the secondary effect of debonding at the final stage.

3.2. Steel-to-concrete bonded joints

The maximum load carrying capacity of EBR joints strengthened with steel plates were 70.14 and 68.97 kN for the two repetitions (Table 2). Steel-strengthened EBROG joints demonstrated a significant increase in the load capacity. Specimens "EBROG-10 × 10-steel-1" and "EBROG-10 × 10-steel-2," reached maximum loads of 84.73 and 90.72 kN, respectively, which indicated 1.22 and 1.30 factors compared to that of EBR joints. Although the EBROG method improved the bond resistance of steel-to-concrete joints, it was not as efficient as that of FRP-to-concrete joints. This may be attributed to an inadequate bond length of the tested joints. The slip distribution and the load-slip behavior of steel-to-concrete bonded joints are plotted in Fig. 9 and Fig. 10, respectively. It can be observed that the load-slip behavior did not experience a horizontal branch, which sparked the assumption that the full capacity was not reached. This can be attributed to that that the used bond length may be less than the effective bond length. The slip distribution that is shown in Fig. 9 demonstrates that the whole bond length experienced slips from the first stages. Since the slip is not zero along the complete bond length, it means that the effective bond length is longer than the used bond length. If the bond length was long enough, the maximum load capacity could go higher, and the effect of the EBROG method could be better perceived. However, more tests and investigations are needed to confirm this hypothesis.

The failure mode of steel-strengthened specimens is demonstrated in Fig. 11. The EBR method resulted in debonding in the concrete substrate. The EBROG joints' failure mode was different for the two repetitions. Specimen "EBROG-10 × 10-steel-1" exhibited debonding, partially in the adhesive layer and partially in the interface between the steel and the adhesive. On the other hand, specimen "EBROG-10 × 10-steel-2" experienced debonding in a deep layer of concrete substrate beneath the grooves. While deep grooves of 10 mm depth were cut in this specimen, debonding occurred completely under the grooves, and the upper surface of the concrete block totally cracked through an explosive failure.

3.3. Discussion on the side-view measurement in steel-to-concrete joint

To assess the stress/strain distribution underneath the bond in the EBROG method, the side-view measurement was performed in specimen number 11. Major strains in several load stages are exhibited in Fig. 12. These graphs present the crack propagation that occurs during loading. It was observed that a crack parallel to the load direction developed near the strip at the loaded end in the EBROG method. Several additional inclined cracks were produced underneath the strip in the concrete depth and grew inside the substrate. These cracks in the EBROG method were deeper than, or equal to the groove depth. Several deep inclined cracks developed as the loading continued, which finally merged at the ultimate stage when the failure happened.

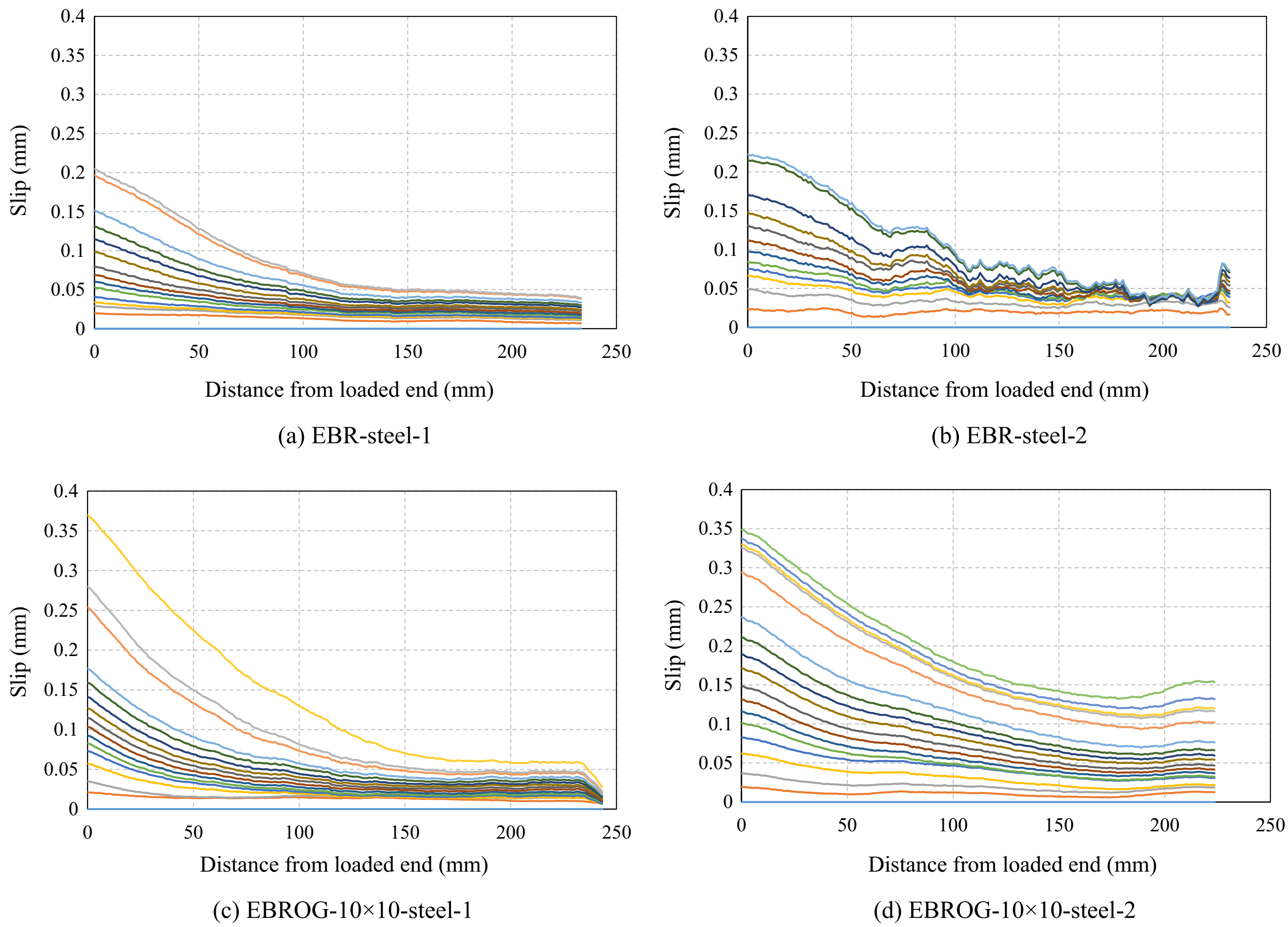

Fig. 9. Slip distribution of steel-to-concrete bonded joints.

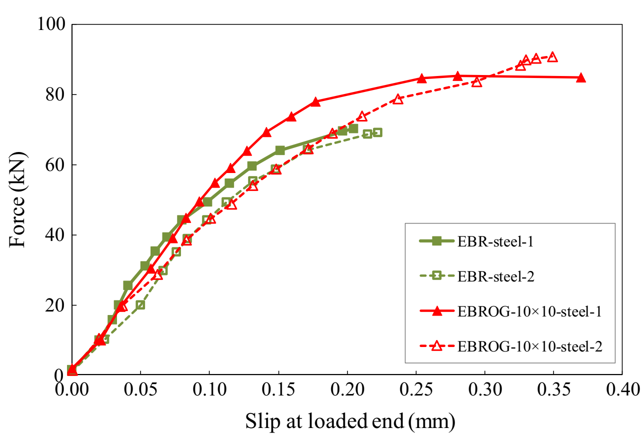

Fig. 10. Load-slip behavior of steel-to-concrete bonded joints.

4. Experimental-analytical model for the EBROG method in the case of cohesive failure

A semi-experimental-analytical model is proposed to determine the bond strength of the FRP-to-concrete EBROG joint if cohesive failure happens. In this model, the maximum bond capacity of pre-cured CFRP strips-to-concrete that is attached by using the EBROG method is evaluated. To better assess the proposed model, experiments that were presented in a paper by authors were also used. All the specimens and their characteristics are shown in Table 3 [29,30].

As discussed before, the failure mode of the EBROG joints were debonding of the FRP strips through the adhesive layer. As the failure plane was inside the adhesive layer, the mechanical properties of the adhesive play an important role in the bond capacity. The maximum interfacial shear stress that could be developed in the adhesive is determined as follows [35,36]:

$$\tau_{max} = 0.9\, f_{u,adhesive} \tag{1}$$

where $f_{u,adhesive}$ is the tensile strength of the epoxy adhesive. Considering the adhesive tensile strength equal to $f_{u,adhesive}$ = 15 MPa for the adhesive used in this research, the maximum interfacial shear stress is determined as $\tau_{max} = 13.5$ MPa. The fracture energy (G_f) of the bond can be determined through the following equation:

$$G_f = \frac{1}{2}\tau_{max} \cdot s_{max} (\text{only if cohesive failure mode happens.}) \tag{2}$$

where s_{max} is the maximum slip at the loaded end at the stage of initiation of debonding. This value was measured in each test and was used to calculate the fracture energy. The fracture energy is the area under the interfacial shear stress-slip (i.e., the bond-slip) relation. Different bond-slip relationships that have equal fracture energy result in identical bond strength. Fracture energy depends on the groove dimensions, concrete compressive strength, etc. and has to be determined in lap-shear tests. Incorporating the fracture energy

(a) “EBR-steel-1” (b) “EBR-steel-2”

(c) “EBROG-10×10-steel-1” (d) “EBROG-10×10-steel-2”

Fig. 11. Failure mode of steel-to-concrete bonded joints.

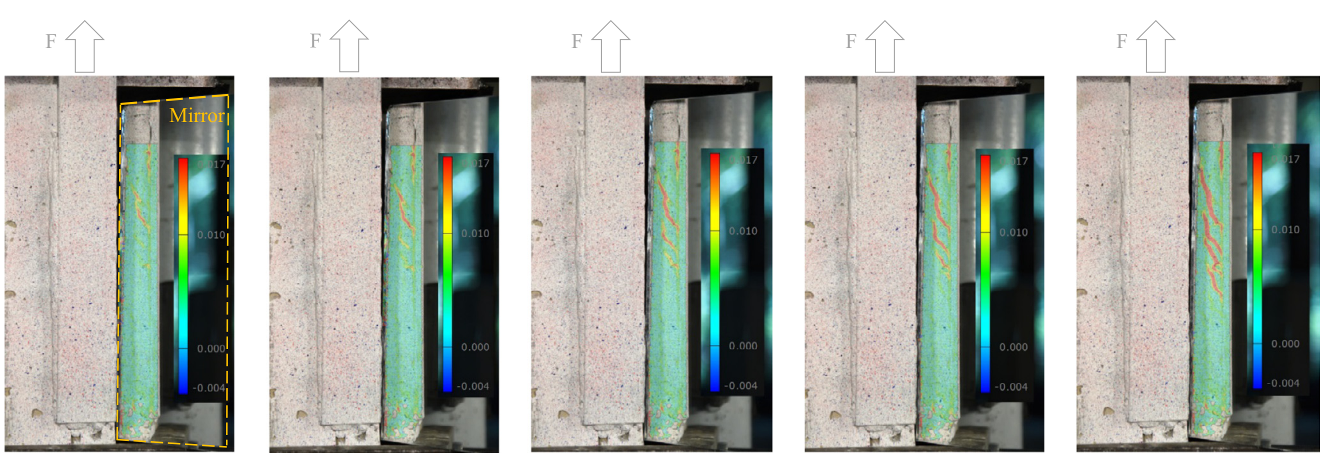

0.91 P_{max} 0.93 P_{max} 0.96 P_{max} 0.98 P_{max} P_{max}

Fig. 12. Crack propagation in the side-view measurement on the steel-to-concrete EBROG joint.

in the following well-known equation [37,38] can predict the bond strength of EBROG joints:

$$P_{u,Theo.} = b_f \sqrt{2G_f E_f t_f} \quad (3)$$

where b_f, t_f and E_f, are the strip width, thickness, and elastic modulus. It is worth mentioning that the above equation demonstrates the maximum force for the bond lengths equal to or longer than the effective bond length. The bond strengths were determined by the

Table 3
Test specimens used for the experimental-analytical model (partly presented here and in [30]).

Specimen label	Number of grooves	Groove width, b_g (mm)	Groove depth, h_g (mm)	$f_c^{'}$ (MPa)	E_f (MPa)	b_f (mm)	t_f(mm)	$E_{adhesive}$ (MPa)
EBROG-5 × 5-1	2	5	5	38.2	165,000	50	1.4	4300
EBROG-5 × 5-2	2	5	5	38.2	165,000	50	1.4	4300
EBROG-10 × 5-1	2	10	5	38.2	165,000	50	1.4	4300
EBROG-10 × 5-2	2	10	5	38.2	165,000	50	1.4	4300
EBROG-5 × 10-1	2	5	10	38.2	165,000	50	1.4	4300
EBROG-5 × 10-2	2	5	10	38.2	165,000	50	1.4	4300
EBROG-10 × 10-1	2	10	10	38.2	165,000	50	1.4	4300
EBROG-10 × 10-2	2	10	10	38.2	165,000	50	1.4	4300

Notes: $f_c^{'}$ = Cylindrical concrete compressive (MPa).

Table 4
Results of the proposed experimental-analytical model.

Specimen label	$f_{u,adhesive}$ (MPa)	τ_{max} (MPa)	s_{max} (mm)	G_f*Notes:* (N/mm)	$P_{u,Theo.}$ (kN)	$P_{u,Exp.}$ (kN)	Ratio $P_{u,Theo.}/P_{u,Exp.}$
EBROG-5 × 5-1	15	13.5	0.38	2.6	54.4	47.1	1.16
EBROG-5 × 5-2*	15	13.5	–	–	–	–	–
EBROG-10 × 5-1	15	13.5	0.27	1.8	45.9	45.0	1.02
EBROG-10 × 5-2	15	13.5	0.29	2.0	47.5	44.6	1.07
EBROG-5 × 10-1	15	13.5	0.4	2.7	55.8	52.7	1.06
EBROG-5 × 10-2	15	13.5	0.36	2.4	53.0	51.4	1.03
EBROG-10 × 10-1	15	13.5	0.72	4.9	74.9	66.7	1.12
EBROG-10 × 10-2	15	13.5	0.82	5.5	80.0	77.7	1.03

Notes: *Data were removed due to premature failure in the clamps during the test (full capacity could not be reached).

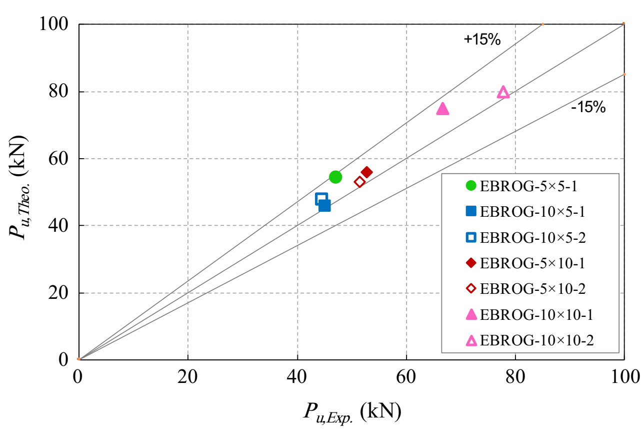

Fig. 13. Comparison of the predicted bond resistance with the experiment.

model, and their comparison to the experimental values are reported in Table 4. The analytical and experimental bond strengths are demonstrated in Fig. 13. It can be observed that the model predicted the bond strengths of FRP strips-to-concrete very well. It is worth mentioning that to be able to propose a versatile model that considers the effect of different parameters, further investigation is needed.

5. Conclusion

The bond behavior of precured CFRP strips and steel plates to concrete was experimentally assessed in this research. Eleven single lap shear tests were performed to compare the effects of using the EBR and EBROG methods on the bond resistance and the slip and strain distribution. Side-view measurements for the EBROG method were conducted for the first time to evaluate the strain distribution beneath the strip. Furthermore, an experimental-analytical model was proposed to predict the bond strength of CFRP-to-concrete EBROG joints. The main conclusions can be summarized as follows:

1 The experimental results showed that the EBROG method tremendously increased the bond strength of FRP to concrete. Using the EBROG method with two longitudinal grooves improved the maximum load capacity two-fold to that of the EBR method. The EBROG method with 5 × 5 mm groove cross section led to a factor of 1.92 in bond strength over the EBR method; and the EBROG method with 5 × 10 mm groove cross section led to factors of 2.15 and 2.10 for two repetitions. The bond resistance of steel to concrete also increased significantly by using the EBROG method. However, it was not as efficient as in the FRP-to-concrete joints.
2 The effective bond length for FRP-strengthened specimens was significantly increased by using the EBROG method. The groove dimensions of 5 × 5 mm and 5 × 10 mm resulted in effective bond lengths equal to 145 and 160 mm, respectively, while it was 90 mm for the EBR method (however, with a lower load).
3 By inspecting the failure modes, it was concluded that in contrast to the EBR joints, CFRP-strengthened EBROG joints experienced debonding in the adhesive layer. The EBROG method stiffened the concrete substrate and helped to postpone the debonding.
4 Considering the failure mode of FRP-strengthened EBROG joints, an experimental-analytical model was proposed to evaluate the bond strength of FRP strips attached to concrete by using the EBROG method, for the first time. Very good agreement between the predicted and experimental bond strengths was observed.
5 By monitoring the crack propagation beneath the concrete substrate in the EBROG method, it was demonstrated that during debonding, the cracks were developed beneath the groove in the steel-to-concrete joint.

Declaration of Competing Interest

There is no conflict of interest.

Acknowledgments

The authors would like to sincerely thank their team members and colleagues at the Structural Engineering Laboratory of Isfahan University of Technology (IUT). Research mobility grants received from Iranian Ministry of Science, Research and Technology (MSRT), Iranian National Elites Foundation, Empa Structural Engineering Research Laboratory (Switzerland), and ZHAW (Swiss Leading House for research collaboration with partner institutions) for the visiting research period of the second author at Empa are greatly acknowledged. This research was also partially funded by the Iran National Science Foundation (INSF) under number 96004203.

References

[1] J.F. Chen, J.G. Teng, Anchorage strength models for FRP and steel plates bonded to concrete, J. Struct. Eng. 127 (7) (2001) 784–791.
[2] X. Lu, J. Teng, L. Ye, J. Jiang, Bond–slip models for FRP sheets/plates bonded to concrete, Eng. Struct. 27 (6) (2005) 920–937.
[3] L. Bizindavyi, K. Neale, Transfer lengths and bond strengths for composites bonded to concrete, J. Compos. Constr. 3 (4) (1999) 153–160.
[4] M.J. Chajes, W.W. Finch, T.F. Januszka, T.A. Thomson, Bond and force transfer of composite material plates bonded to concrete, ACI Struct. J. 93 (2) (1996) 208–217.
[5] Y.-W. Zhou, Y.-F. Wu, Y. Yun, Analytical modeling of the bond–slip relationship at FRP-concrete interfaces for adhesively-bonded joints, Compos. B Eng. 41 (6) (2010) 423–433.
[6] J. Yao, J. Teng, J.F. Chen, Experimental study on FRP-to-concrete bonded joints, Compos. B Eng. 36 (2) (2005) 99–113.
[7] T.H.-K. Kang, J. Howell, S. Kim, D.J. Lee, A state-of-the-art review on debonding failures of FRP laminates externally adhered to concrete, Int. J. Concr. Struct. Mater. 6 (2) (2012) 123–134.
[8] M. Perrella, V.P. Berardi, G. Cricrì, A novel methodology for shear cohesive law identification of bonded reinforcements, Compos. B Eng. 144 (2018) 126–133.
[9] E. Martinelli, A. Caggiano, A unified theoretical model for the monotonic and cyclic response of FRP strips glued to concrete, Polymers 6 (2) (2014) 370–381.
[10] D. Mostofinejad, K. Sanginabadi, M.R. Eftekhar, Effects of coarse aggregate volume on CFRP-concrete bond strength and behavior, Constr. Build. Mater. 198 (2019) 42–57.
[11] American Concrete Institute (ACI), ACI 440.2R-08, Guide for the Design and Construction of Externally Bonded FRP Systems for Strengthening Concrete Structures, Farmington Hills, MI, 2008.
[12] R. Seracino, M. Raizal Saifulnaz, D. Oehlers, Generic debonding resistance of EB and NSM plate-to-concrete joints, J. Compos. Constr. 11 (1) (2007) 62–70.
[13] Standards Australia, HB 305-2008, Design Handbook for RC Structures Retrofitted with FRP and Metal Plates: Beams and Slabs, Sydney, NSW, Australia, 2008.
[14] D. Mostofinejad, E. Mahmoudabadi, Grooving as alternative method of surface preparation to postpone debonding of FRP laminates in concrete beams, J. Compos. Constr. 14 (6) (2010) 804–811.
[15] D. Mostofinejad, S.M. Shameli, Externally bonded reinforcement in grooves (EBRIG) technique to postpone debonding of FRP sheets in strengthened concrete beams, Constr. Build. Mater. 38 (2013) 751–758.
[16] N. Moshiri, A. Hosseini, D. Mostofinejad, Strengthening of RC columns by longitudinal CFRP sheets: effect of strengthening technique, Constr. Build. Mater. 79 (2015) 318–325.
[17] D. Mostofinejad, N. Moshiri, Compressive strength of CFRP composites used for strengthening of RC columns: comparative evaluation of EBR and grooving methods, J. Compos. Constr. 19 (5) (2014) 04014079.
[18] D. Mostofinejad, A. Torabian, Experimental study of circular RC columns strengthened with longitudinal CFRP composites under eccentric loading: comparative evaluation of EBR and EBROG methods, J. Compos. Constr. 20 (2) (2015) 04015055.
[19] D. Mostofinejad, A. Akhlaghi, Experimental INVESTIGATION OF THE EFFICacy of EBROG method in seismic rehabilitation of deficient reinforced concrete beam-column joints using CFRP sheets, J. Compos. Constr. 21 (4) (2016) 04016116.
[20] D. Mostofinejad, M. Hajrasouliha, 3D beam–column corner joints retrofitted with X-shaped FRP sheets attached via the EBROG technique, Eng. Struct. 183 (2019) 987–998.
[21] D. Mostofinejad, A.T. Kashani, Experimental study on effect of EBR and EBROG methods on debonding of FRP sheets used for shear strengthening of RC beams, Compos. B Eng. 45 (1) (2013) 1704–1713.
[22] M. Ghorbani, D. Mostofinejad, A. Hosseini, Bond behavior of CFRP sheets attached to concrete through EBR and EBROG joints subject to mixed-mode I/II loading, J. Compos. Constr. 21 (5) (2017) 04017034.
[23] A. Hosseini, D. Mostofinejad, Effect of groove characteristics on CFRP-to-concrete bond behavior of EBROG joints: experimental study using particle image velocimetry (PIV), Constr. Build. Mater. 49 (2013) 364–373.
[24] D. Mostofinejad, M.H. Mofrad, A. Hosseini, H.H. Mofrad, Investigating the effects of concrete compressive strength, CFRP thickness and groove depth on CFRP-concrete bond strength of EBROG joints, Constr. Build. Mater. 189 (2018) 323–337.
[25] A. Tajmir-Riahi, N. Moshiri, D. Mostofinejad, Bond mechanism of EBROG method using a single groove to attach CFRP sheets on concrete, Constr. Build. Mater. 197 (2019) 693–704.
[26] A. Moghaddas, D. Mostofinejad, E. Ilia, Empirical FRP-concrete effective bond length model for externally bonded reinforcement on the grooves, Compos. Part B: Eng. (2019).
[27] A. Moghaddas, D. Mostofinejad, Empirical FRP-concrete bond strength model for externally bonded reinforcement on grooves, J. Compos. Constr. 23 (2) (2018) 04018080.
[28] A. Tajmir-Riahi, D. Mostofinejad, N. Moshiri, Bond resistance of a single groove in EBROG method to attach CFRP sheets on concrete, in: Proceedings of the Ninth International Conference on Fibre-Reinforced Polymer (FRP) Composites in Civil Engineering (CICE 2018), Paris, France, 2018, pp. 368–373.
[29] N. Moshiri, D. Mostofinejad, A. Tajmir-Riahi, Bond behavior of pre-cured CFRP strips to concrete using externally bonded reinforcement on groove (EBROG) method, in: Proceedings of the Ninth International Conference on Fibre-Reinforced Polymer (FRP) Composites in Civil Engineering (CICE 2018), Paris, France, 2018, pp. 361–367.
[30] N. Moshiri, A. Tajmir-Riahi, D. Mostofinejad, C. Czaderski, M. Motavalli, Experimental and analytical study on CFRP strips-to-concrete bonded joints using EBROG method, Compos. B Eng. 158 (2019) 437–447.
[31] ASTM E8/E8M-13Standard Test Methods for Tension Testing of Metallic Materials, ASTM International, West Conshohocken, PA, 2013. 10.1520/E0008_E0008M-13.
[32] ASTM D3039/D3039M, Standard Test Method for Tensile Properties of Polymer Matrix Composite Materials; 2000.
[33] A. Tajmir-Riahi, N. Moshiri, D. Mostofinejad, Inquiry into bond behavior of CFRP sheets to concrete exposed to elevated temperatures – Experimental & analytical evaluation, Compos. B Eng. 173 (2019) 106897.
[34] A. Hosseini, D. Mostofinejad, M. Hajialilue-Bonab, Displacement and strain field measurement in steel and RC beams using particle image velocimetry, J. Eng. Mech. 140 (11) (2014) 04014086.
[35] D. Fernando, Bond Behaviour and Debonding Failures in CFRP-Strengthened Steel Structures, Department of Civil and Structural Engineering, The Hong Kong Polytechnic University, Hong Kong, China, 2010.
[36] E. Martinelli, A. Hosseini, E. Ghafoori, M. Motavalli, Behavior of prestressed CFRP plates bonded to steel substrate: numerical modeling and experimental validation, Compos. Struct. 207 (2019) 974–984.
[37] C. Czaderski, Strengthening of Reinforced Concrete Members by Prestressed Externally Bonded Reinforcement with Gradient Method Ph.D. Thesis, ETH Zürich, Zürich Switzerland, 2012.
[38] Schweizerischer Ingenieur- und Architektenverein (SIA), SIA166, Klebebewehrungen (Externally bonded reinforcement), Zurich, Switzerland, 2004.